

# Spectral side channels in quantum key distribution under laser damage

Binwu Gao,<sup>1,\*</sup> Junxuan Liu,<sup>1,\*</sup> Ekaterina Borisova,<sup>2,3</sup> Hao Tan,<sup>4</sup> Mingyang Zhong,<sup>1</sup> Zihao Chen,<sup>1</sup> Qingquan Peng,<sup>1</sup> Weixu Shi,<sup>1</sup> Anastasiya Ponomsova,<sup>2,3</sup> Vadim Makarov,<sup>2,3,5</sup> and Anqi Huang<sup>1,†</sup>

<sup>1</sup>College of Computer Science and Technology, National University of Defense Technology, Changsha 410073, People's Republic of China

<sup>2</sup>Russian Quantum Center, Skolkovo, Moscow 121205, Russia

<sup>3</sup>NTI Center for Quantum Communications, National University of Science and Technology MISiS, Moscow 119049, Russia

<sup>4</sup>China Telecom Quantum Information Technology Group Co., Ltd., Hefei 230088, China

<sup>5</sup>Vigo Quantum Communication Center, University of Vigo, Vigo E-36310, Spain

(Dated: December 15, 2025)

In the transmitter of a quantum key distribution (QKD) system, a dense wavelength-division multiplexer (DWDM) is typically used to combine quantum and synchronization signals and is directly connected to the quantum channel. As a result, it becomes the first optical component exposed to laser-injection attacks. Therefore, understanding the behavior of DWDMs under such attacks is essential for assessing the practical security of QKD systems. In this work, we systematically investigate the characteristics of DWDMs under high-power laser illumination. Our experimental results show that certain DWDM samples exhibit pronounced changes in their spectral features once the injected laser power surpasses a specific threshold. Taking the Trojan-horse attack as an illustrative example, we further perform a theoretical analysis of the resulting spectral side channel and show that it can reduce the maximum secure transmission distance to below 66.9% of its original value. By combining experimental observations with theoretical modeling, this study advances the understanding of the influence of DWDMs on the practical security of QKD systems.

## I. INTRODUCTION

Quantum key distribution (QKD) offers information-theoretic security for sharing symmetric keys between two communicating parties, Alice and Bob. Its security stems from the fundamental principles of quantum physics and is therefore immune to advances in computational power [1–4]. However, the physical devices used in practical QKD implementations inevitably deviate from their idealized models, giving rise to security vulnerabilities [5–27]. These device imperfections constitute side channels that may enable an eavesdropper (Eve) to gain information about the secret key.

Considerable effort has been devoted to identifying these vulnerabilities in practical QKD devices and developing corresponding attack strategies. Among all components, single-photon detectors were historically the most vulnerable, and their imperfections have been heavily exploited by various quantum hacking attacks [5–7, 10, 15, 16, 28–34]. Fortunately, the measurement-device-independent (MDI) QKD protocol guarantees that imperfections in measurement devices—including single-photon detectors—do not compromise the overall security of the QKD system [35]. As a result, the security and performance of transmitter modules have become increasingly critical for practical QKD implementations.

In recent years, numerous attacks targeting QKD transmitters have been proposed, including the Trojan-horse attack (THA) [36–40], the laser-seeding attack [14, 19, 41], and the induced-photorefraction attack [42–44].

In these attacks, Eve injects external light to obtain encoding information through back-reflected photons, manipulate the behavior of the laser source, or alter the operational characteristics of phase and intensity modulators. To mitigate such threats, researchers have deployed essential passive optical components—such as attenuators, isolators, and dense wavelength-division multiplexers (DWDMs)—to limit the amount of injected light entering the transmitter, preventing Eve from extracting secret information [20, 39]. However, recent studies have revealed that the attenuation of optical attenuators and the isolation of optical isolators can degrade under high-power optical illumination [20, 24], potentially allowing Eve to revive light-injection attacks and compromise the security of the QKD system.

The DWDM, another widely used passive component, play an important role in a practical QKD system by multiplexing quantum-state pulses and synchronization pulses before transmission through the quantum channel [45–49]. Since the DWDM is directly connected to the quantum channel, it is the first optical device encountered by Eve when launching laser-injection attacks against the QKD transmitter. Therefore, understanding the behavior of DWDMs under such attacks is essential for comprehensively assessing the practical security of QKD systems. Nevertheless, the potential security loopholes introduced by DWDMs have remained largely unexplored.

In this work, we conduct a detailed investigation into the behavior of DWDMs under laser-damage attacks. Our experimental results show that when the injected high-power laser exceeds a certain threshold, its wavelength can shift after passing through specific DWDM samples, leading to the appearance of additional spectral

\* These authors contributed equally

† angelhuang.hn@gmail.com

peaks at the output. This behavior potentially opens opportunities for Eve to exploit. Through further theoretical analysis, we demonstrate that this spectral side channel can reduce the maximum secure transmission distance to below 66.9% of its original value. By combining experimental observations with theoretical modeling, this work uncovers the security implications introduced by DWDMs in practical QKD systems and provides insights for designing more secure QKD transmitters.

The remainder of this paper is organized as follows. Section II describes the experimental setup and measurement procedures for the laser-damage attack on DWDMs. The experimental results are presented in Sec. III. Section IV analyzes the impact of the revealed spectral side channel on QKD security, using the THA as a representative example of light-injection attacks. Finally, Sec. V discusses potential countermeasures and concludes the paper.

## II. TESTING METHOD

The DWDM sample under test has three ports, labeled COM, Ref, and Pass. Alice's quantum-state pulses enters through the Pass port, while the synchronization light enters through the Ref port. The DWDM multiplexes these two types of signals and passes them to the quantum channel through the COM port. To examine the optical behavior of the DWDM under high-power illumination, we inject a high-power laser into the COM port to simulate Eve's light entering from the quantum channel.

Depending on the direction of light propagation through the DWDM, the experiment is divided into two scenarios. In the first scenario, we analyze how the characteristics of the injected high-power laser change after passing through the DWDM and reaching the inside of transmitter. This scenario corresponds to Eve injecting light from the quantum channel and is discussed in detail in the main text. In contrast, the second scenario investigates how the characteristics of light emitted by the transmitter are altered after passing through a DWDM that has been exposed to high-power laser illumination. As this case serves as a complementary analysis, it is presented in Appendix A for clarity and conciseness.

### A. Experimental setup

The experimental setup is shown in Fig. 1. In this setup, a high-power laser (HPL) is connected to the COM port of the DWDM through a 99:1 beam splitter (BS), simulating Eve's injection of high-power laser light from the quantum channel into the transmitter. Optical spectrum analyzer 1 (OSA1), OSA2, and OSA3 are connected to their respective BSs to measure the spectral characteristics. OSA1 monitors the input spectrum at the COM port, while OSA2 and OSA3 record the output spectra at

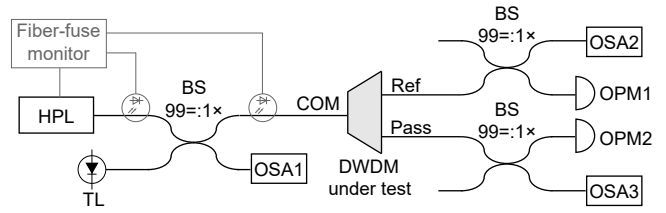


FIG. 1. Schematic diagram of the experimental setup, with the DWDM as a replaceable sample under test. All fibers are standard single mode. OSA, optical spectrum analyzer; OPM, optical power meter; COM, common port; Pass, pass port; Ref, reflect port; TL, tunable laser; HPL, high-power laser; BS, beam splitter. The coupling ratio of the BS denoted  $99 =: 1 \times$  means that 99% of light passes to the port horizontally opposite in the graphical symbol of the BS, while 1% of light is coupled across to the other port.

the Ref and Pass ports, respectively. Optical power meter 1 (OPM1) and OPM2 are used to measure the optical power at the Ref and Pass ports. A tunable laser (TL), which provides a constant-power laser with adjustable wavelength, is also connected to the COM port of the DWDM via a 99:1 BS to characterize the initial spectral response of the DWDM sample. Additionally, to prevent equipment damage caused by fiber fuse events, a fiber fuse monitor is applied in the setup.

### B. Test procedure

Before conducting the main experiment, we first characterize the stability of the HPL, which is the core device used in the laser-damage attack. The HPL provides continuous-wave (c.w.) light with a maximum output power of 10 W, and its stability test is described in detail in Appendix B. After confirming stable output, we proceed with the subsequent measurements. Prior to testing the DWDM samples, we also verify that the rest of the setup—excluding the DWDMs—exhibits no significant changes under high-power illumination. This ensures that any observed changes in the later experiment can be attributed solely to the DWDM sample under test.

A “successfully hacked case” is defined as any instance in which the spectrum of the light exhibits significant differences before and after passing through the DWDM. Before enabling high-power illumination, we switch off the HPL and turn on the TL to measure the initial spectral characteristics of the DWDM sample. The tuning range of the TL is determined by the central wavelength and channel passband of each DWDM sample. To obtain the complete initial spectrum, the TL must sweep across the full operating wavelength range of the DWDM. For example, for a DWDM with the central wavelength of 1550.12 nm and the passband of  $\pm 0.11$  nm, the TL is swept from 1548 nm to 1552 nm in 20 pm increments, illuminating the device for 3 seconds at each step. During this sweep, OSA2 and OSA3 operate in hold-max mode,

TABLE I. The detailed parameters of the DWDM samples to be tested in the experiment

Type	Sample	Central Wavelength(nm)	Manufacturer
DWDM1	1,2	1550.12	A
DWDM2	3,4	1550.12	A
DWDM3	5,6	1549.32	A

with a scan speed of 200 nm/s and a sampling resolution of 2 pm, thereby recording the maximum response at each wavelength and yielding the initial spectral profile of the DWDM.

Afterward, the TL is turned off and the HPL is turned on. OSA2 and OSA3 are switched to live mode to record the real-time spectrum during the laser-damage attack. The HPL power starts at 1 W and increases in increments of approximately 1 W, with continuous illumination of up to 10 minutes at each level. If the spectrum observed on OSA2 or OSA3 satisfies the previously defined criteria for a successfully hacked case, the experiment is immediately terminated. If the HPL reaches its maximum output of 10 W without causing notable spectral changes, the experiment is also concluded.

### III. TESTING RESULTS

#### A. Spectral feature under test

Three types of DWDMs (DWDM1–3) were tested in the experiment, and two independent samples were evaluated for each type to ensure experimental reliability. The detailed parameters of all DWDM samples are listed in Table I. The experimental procedures followed the methods described in Sec. II. Among the three types of DWDMs, only DWDM1 exhibited successfully hacked cases as defined in Sec. II. Furthermore, for each DWDM type, the two independent samples produced consistent test results. In the following, we present the detailed experimental results of sample 1 as a representative of the DWDM1 type. Since sample 2 showed similar behavior, its results are summarized only briefly. Samples 3 and 5 are then used as the representatives of DWDM2 and DWDM3, respectively.

Figures 2(a) and (b) show the spectra at the Pass and Ref ports of sample 1 in the absence of the laser-damage attack. The initial spectrum confirms that both the central wavelength and the channel passband of the DWDM are consistent with the specifications provided in the manufacturer’s datasheet.

Figure 3 shows the spectral response of the DWDM under the laser-damage attack. At the HPL power of 1 W, as shown in Fig. 3(a) and (b), the Pass-port output exhibits only a reduction in optical power compared to the input at the COM port. The spectral shape at the Ref port remains nearly unchanged and closely matches

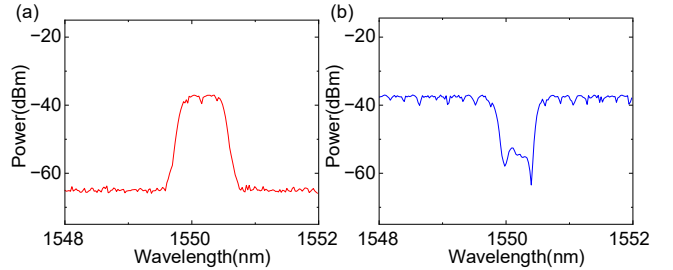


FIG. 2. The initial spectral of sample 1. (a) Output spectrum at the Pass port. (b) Output spectrum at the Ref port.

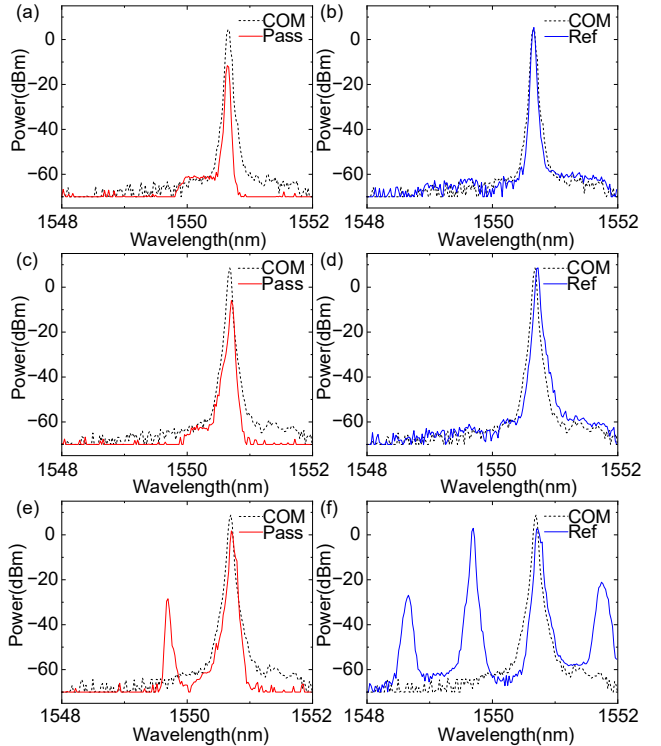


FIG. 3. The experimental spectral results for sample 1. The black dashed line represents the input spectrum at the COM port, measured by OSA1. The red and blue solid lines represent the output spectra at the Pass and Ref ports, measured by OSA3 and OSA2, respectively. (a) and (b) show the experimental spectral results when the HPL power is 1 W; (c) and (d) correspond to the results at 4 W; and (e) and (f) present the results at 5 W.

the input spectrum. The output wavelengths at both ports coincide with the high-power laser wavelength of approximately 1550.7 nm. Although the Pass port is not designed to transmit light at this wavelength, a small fraction of the incident light still leaks through due to the limited isolation of the DWDM, which is expected. When the HPL power is increased to 4 W, the output spectra remain qualitatively similar to those observed at 1 W, as shown in Fig. 3(c) and (d). The main differences are an increase in output power and a broader spectral shape, consistent with the spectral characteristics of the

HPL at this power level.

A striking change occurs when the HPL power reaches 5 W. As shown by the dashed curve in Fig. 3(e), the spectrum at the COM port still exhibits a single peak at 1550.7 nm, indicating that the wavelength of the injected laser remains stable. In contrast, the spectra at both the Pass and Ref ports undergo significant changes, with additional peaks emerging at wavelengths different from 1550.7 nm. Specifically, as illustrated by the solid curve in Fig. 3(e), besides the original peak at 1550.7 nm, a new peak appears near 1549.7 nm. Figure 3(f) further shows that four notable peaks appear between 1548 nm and 1552 nm, located at approximately 1548.7 nm, 1549.7 nm, 1550.7 nm, and 1551.7 nm, spaced by roughly 1 nm. The peaks near 1549.7 nm and 1550.7 nm are the strongest, while the others are weaker and symmetrically distributed.

For samples 2, 3, and 5, the initial spectra are not illustrated here because all of them are consistent with the specifications stated in their datasheets. Figure 4 shows the input and output spectra of sample 2 under HPL powers of 1 W and 6 W. When the HPL power reaches 6 W, sample 2 exhibits the same phenomenon observed in sample 1 — multiple spectral peaks appear in the outputs from both the Pass and Ref ports, as illustrated in Fig. 4(c) and (d). For samples 3 and 5, measurements were performed with HPL powers ranging from 1 W up to the maximum of 10 W. In these tests, no significant multi-peak features were observed, and therefore we present only the results at the maximum HPL power of 10 W. Figure 5 shows the input and output spectra of samples 3 and 5 under this condition. Compared with the input spectrum at the COM port, the output at the Pass port only shows a reduction in power, while the output at the Ref port remains essentially unchanged. These results indicate that both samples retain their normal spectral characteristics under illumination by the 10 W high-power laser, with no noticeable spectral distortions or abnormal features.

Our experimental results show that the samples of DWDM1 exhibit significant spectral changes when subjected to the laser-damage attack. In particular, the wavelength of the transmitted high-power laser shifts, resulting in a multi-peak structure in the output spectrum. In contrast, the samples of DWDM2 and DWDM3 do not display this behavior. Even when the HPL power reaches 10 W, their output spectra remain unchanged and no multi-peak features are observed.

## B. Possible mechanism

The experiment on DWDM1 shows that when the injected high-power laser reaches a sufficiently high level, its wavelength changes after passing through the DWDM, producing a multi-peak structure in the spectra observed at both the Pass and Ref ports. The wavelengths of these newly appeared peaks differ from that of the inci-

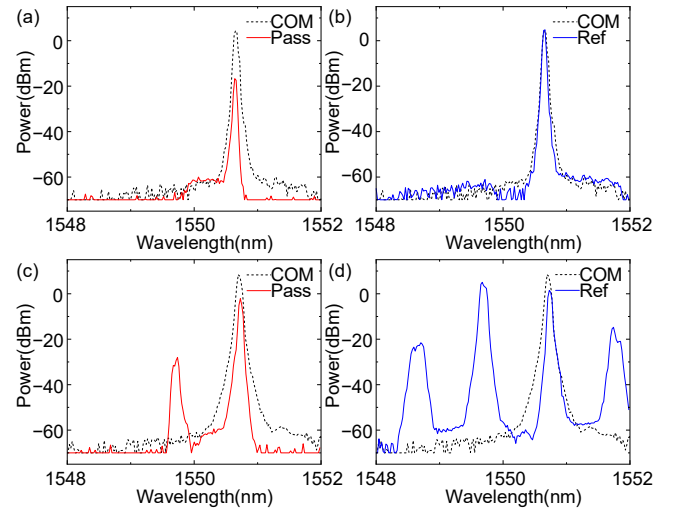


FIG. 4. The experimental spectral results for sample 2. The black dashed line represents the input spectrum at the COM port, measured by OSA1. The red and blue solid lines represent the output spectra at the Pass and Ref ports, measured by OSA3 and OSA2, respectively. (a) and (b) show the experimental spectral results when the HPL power is 1 W, while (c) and (d) present the results at an HPL power of 6 W.

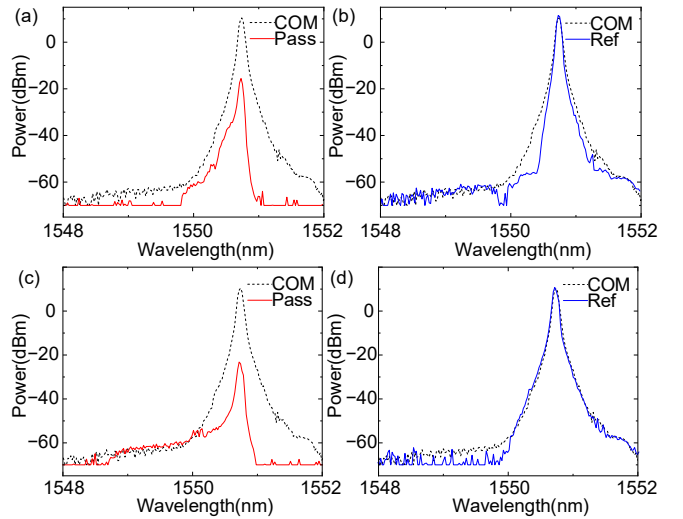


FIG. 5. The experimental spectral results for samples 3 and 5. The black dashed line represents the input spectrum at the COM port, measured by OSA1. The red and blue solid lines represent the output spectra at the Pass and Ref ports, measured by OSA3 and OSA2, respectively. (a) and (b) show the experimental spectral results of sample 3 under the HPL power of 10 W, while (c) and (d) present the corresponding results for sample 5 at the same power level.

dent high-power laser, indicating that the laser-damaged DWDM splits the high-power input into multiple wavelength components. In addition, the power of these components depends on wavelength, i.e., the peak closest to the original wavelength has the highest power, while the

others are weaker and symmetrically distributed around it.

Because the information about the mechanism of DWDM1 is quite limited from the manufacture, we cannot provide a conclusive explanation for this phenomenon. It is worth noting, however, that the wavelengths at which the new peaks appear follow a regular pattern, with approximately one peak every 1 nm. This behavior closely resembles the spectrum of an optical frequency comb. We therefore hypothesize that, due to particular characteristics of the fabrication process, this DWDM sample undergoes a nonlinear optical effect — possibly four-wave mixing — when illuminated by high-power laser light. Such a process broadens the initially single-wavelength input into a comb-like spectrum, giving rise to the observed multi-peak features.

#### IV. SECURITY ANALYSIS

The experimental results presented in Sec. III demonstrate that laser-damage attack on the DWDM may introduce spectral side channel that could be exploited by Eve to implement light-injection attacks. In this section, we analyze the additional security threats this spectral side channel may introduce to practical QKD systems, using the THA as a case study.

In THA, Eve sends Trojan-horse photons along the quantum channel to the transmitter. A portion of Trojan-horse photons is encoded with key information and then reflected back to Eve. Eve extracts encoding information from the Trojan-horse photons reflected back to her, thereby compromising the security of the QKD system [36–40]. As noted in Ref [39], the amount of information that Eve can extract from the source is directly influenced by the number of Trojan-horse photons reflected back to her. This number depends on three main factors—the intensity of the Trojan-horse light injected into the transmitter, the isolation provided within the transmitter, and the internal reflectivity of its components.

The Trojan-horse light injected by Eve from the quantum channel into the transmitter, after passing through the DWDM and heading towards the encoding module, can be observed from our experimental results as shown in Fig. 3. To evaluate the transmitter’s isolation against Trojan-horse light, we adopt the methodology outlined in Ref. [50] for measuring the isolation of attenuators and isolators. Detailed procedures are provided in Appendix C. Furthermore, we pessimistically assume an internal reflection efficiency of 1 at the transmitter, representing the most favorable scenario for Eve.

We utilize the theoretical framework for security analysis outlined in Refs. [39, 40] to quantitatively analyze the impact of THA on the security of QKD systems. Specifically, in this work, we analyzed the impact of the combined laser-damage and THA attacks on the security key rate of weak + vacuum decoy-state BB84 QKD proto-

col [51]. Based on Ref. [52], the key generation rate with weak coherent source (WCS) can be expressed as

$$R \geq q\{-Q_\mu H_2(E_\mu)f(E_\mu) + P_1 Y_1^\mu [1 - H_2(e_1^\mu)]\}. \quad (1)$$

Here,  $q$  depends on the specific protocol, for instance,  $q = 0.5$  for the typical BB84 protocol;  $\mu$  represents the average photon number of signal state;  $Q_\mu$  and  $E_\mu$  respectively represent the total gain and error rate of the signal state;  $Y_1^\mu$  and  $e_1^\mu$  are the yield and error rate of single-photon pulses;  $P_1$  is the probability of single-photon pulses;  $f(x)$  is the bidirectional error correction efficiency, and  $H_2(x) = -x \log_2(x) - (1-x) \log_2(1-x)$  is the binary Shannon information entropy.

In Eq.(1),  $Q_\mu$  and  $E_\mu$  can be calculated by communicating parties. Therefore, to assess the lower bound of the key rate, we should estimate the lower bound of  $Y_1^\mu$  and the upper bound of  $e_1^\mu$ . Reference [51] provides the expressions for  $Y_1^\mu$  and  $e_1^\mu$  in the absence of THA as follows.

$$Y_1^\mu \geq Y_1^{\mu,L} = \frac{\mu}{\mu\nu - \nu^2} \left( Q_\nu e^\nu - Q_\mu e^\mu \nu^2 - \frac{\mu^2 - \nu^2}{\mu^2} Y_0 \right),$$

$$e_1^\mu \leq \frac{E_\nu Q_\nu e^\nu - e_0 Y_0}{Y_1^{\mu,L} \nu}. \quad (2)$$

Here,  $\mu$  ( $\nu$ ) represents the average photon number of signal state (decoy state);  $Q_\mu$  and  $E_\mu$  ( $Q_\nu$  and  $E_\nu$ ) respectively represent the total gain and error rate of signal state (decoy state);  $Y_0$  ( $e_0$ ) is dark count rate (dark error rate).

However, Eve’s THA creates a discrepancy between phase errors and bit errors. Reference [39], building on the GLLP framework [52, 53], derived the specific expression for parameter  $e_1^\mu$  under the influence of THA as follows.

$$e_1^\mu = e_{1,\overline{THA}}^\mu + 4\Delta'(1 - \Delta')(1 - 2e_{1,\overline{THA}}^\mu)$$

$$+ 4(1 - 2\Delta')\sqrt{\Delta'(1 - \Delta')}e_{1,\overline{THA}}^\mu(1 - e_{1,\overline{THA}}^\mu),$$

$$\Delta' = \frac{\Delta}{Y_1^\mu},$$

$$\Delta = \frac{1}{2} [1 - \exp(-\mu_{\text{out}}) \cos(\mu_{\text{out}})]. \quad (3)$$

Here,  $\mu_{\text{out}}$  represent the intensity of the Trojan-horse light, and  $\Delta$  represents the probability of Alice measuring the quantum coin in the basis X and obtaining the quantum state  $|1_X\rangle$ . Further details about  $\Delta$  and  $\Delta'$  can be found in Ref. [39].

According to Ref. [40], THA can learn not only phase-encoded information but also intensity-encoded information, making the signal and decoy states distinguishable. It also suggests using trace distance to quantitatively characterize the distinguishability of Trojan-horse photons on signal and decoy states, with the formula being

$$|Y_1^\mu - Y_1^\nu| \leq D_{\mu,\nu},$$

$$|Y_1^\mu e_1^\mu - Y_1^\nu e_1^\nu| \leq D_{\mu,\nu}. \quad (4)$$

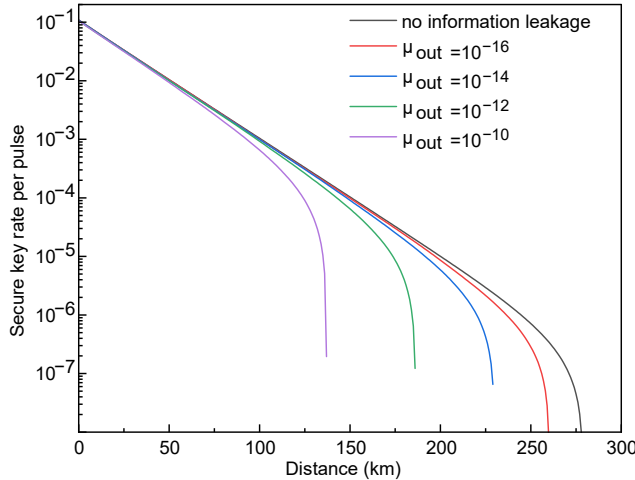


FIG. 6. Key rate under different intensities of Trojan-horse photons. The main parameters used in the simulation are as follows. Fiber loss coefficient of 0.2 dB/km, Bob's detector detection efficiency of 42%, optical error rate of 1%, dark count probability per gate of  $8 \times 10^{-8}$ , bidirectional error correction efficiency of 1.16 and dark error rate  $e_0$  of 0.5.

$D_{\mu,\nu}$  is the trace distance between probability distributions arising from the signal state and the decoy state. Based on Ref. [17], one can estimate the lower bound of  $Y_1^\mu$  and the upper bound of  $e_1^\mu$  under the risks of distinguishable decoy state. Subsequently, by integrating Eq.(1)-(3), one can estimate the key rate under the influence of THA. Figure 6 depicts the curve of the secure key rate under different intensities of Trojan-horse photons.

We integrate the Pass port results of the sample 1 from the experiment (Fig. 3(e)) with the security theoretical model to quantitatively evaluate the maximum key generation distance across different wavelengths. When Trojan-horse photons pass through the DWDM, the wavelengths of some photons change, i.e., a significant number of photons appear at 1549.7 nm and 1550.7 nm. Given that 1550.7 nm corresponds to the original Trojan-horse wavelength, the key concern lies in the additional vulnerabilities caused by the spectral side channel. Thus, the subsequent analysis focuses on its impact—particularly that of the Trojan-horse photons at 1549.7 nm—on the practical security of QKD. Using the intensity conditions of the Trojan-horse laser assumed in Ref. [39], along with our experimental results on the isolation of the isolator, attenuator, and DWDM at different wavelengths, we calculated that the intensity of the Trojan-horse photons is on the order of  $10^{-12}$ . By incorporating this into the theoretical model, the maximum key generation distance is reduced to 66.9% of the one without attack. Figure 7 displays the number of Trojan-horse photons in the frequency domain, along with the corresponding maximum distances of secure keys generation for these photons. Our analysis indicates that the discovered spectral side channel could potentially reduce the maximum distance of secure keys generation, repre-

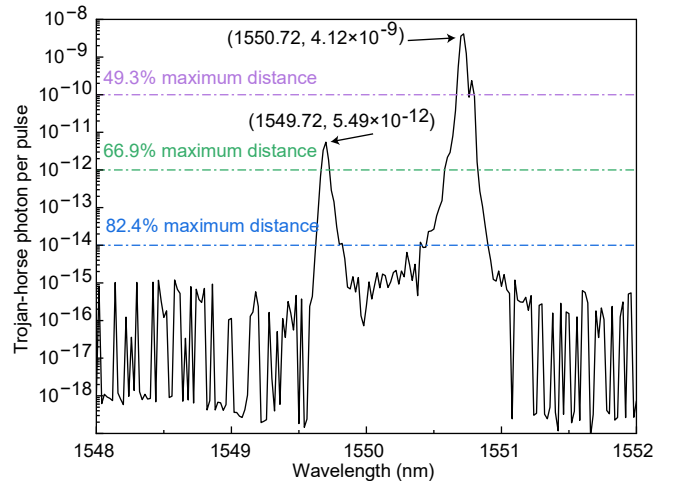


FIG. 7. The number of Trojan-horse photons in the frequency domain, along with the corresponding maximum distances of key generation.

senting a significant security risk.

## V. CONCLUSION

In this paper, we experimentally investigate the effects of laser-damage attack on DWDMs under high-power laser illumination and identify a previously unreported spectral side channel in certain DWDM samples. Our theoretical analysis further reveals that this side channel introduces potential security risks to QKD systems. Specifically, when a laser-damage attack is launched at the transmitter, the DWDM—being the first optical component exposed to the injected light—can cause part of the high-power laser to undergo wavelength changes as it passes through, resulting in multiple peaks in the output spectrum. Using the Trojan-horse attack as a representative example of light-injection attacks, we analyze the impact of this spectral side channel on a decoy-state BB84 QKD system. Our results show that this side channel can reduce the secure key distribution distance to approximately 66.9% of its original value.

Our experimental results and theoretical analysis demonstrate that the spectral side channel constitutes a significant security vulnerability. A potential counter-measure is to place an isolator at the outermost output of the transmitter, directly interfacing with the quantum channel. This configuration can block a substantial portion of Eve's injected high-power light and thereby prevent the DWDM from being directly exposed. It is worth noting that Ref. [24] reports that isolators themselves may also be affected by laser-damage attacks, leading to changes in their characteristics, and suggests that incorporating additional isolators can protect the remaining components of the QKD source against light-injection attacks. Therefore, deploying multiple isolators between the DWDM and the quantum channel is an effective

approach to prevent the DWDM from being damaged, thereby enhancing the practical security of the QKD system. This study offers valuable guidance for designing and implementing more robust QKD systems. Future work could focus on clarifying the mechanism behind the multi-peak phenomenon in DWDMs under the laser-damage attack.

## ACKNOWLEDGMENTS

**Funding:** Quantum Science and Technology-National Science and Technology Major Project (2021ZD0300704) and National Natural Science Foundation of China (62371459). V.M. acknowledges funding from the Galician Regional Government (consolidation of research units: atlanTTic and own funding through the “Planes Complementarios de I+D+I con las Comunidades Autónomas” in Quantum Communication), MICIN with funding from the European Union NextGenerationEU (PRTR-C17.I1), and the “Hub Nacional de Excelencia en Comunicaciones Cuánticas” funded by the Spanish Ministry for Digital Transformation and the Public Service and the European Union NextGenerationEU.

## Appendix A: Experimental details of light emitted from the transmitter under the laser-damage attack on the DWDM

In the main text, we investigated how high-power laser injected from the quantum channel is altered after passing through the DWDM located at the transmitter side. In this appendix, as a complementary study, we examine how the light emitted from the transmitter is modified after propagating through a DWDM that has been subjected to the laser-damage attack. These two scenarios are complementary and together provide a systematic assessment of the impact of laser-damage attacks on the practical security of QKD systems employing DWDM components.

### 1. Setup and test procedure

The experiment setup is shown in Fig. 8. It is noteworthy that this experiment considers the practical application scenarios of the QKD system, focusing on the transmittance of DWDM for specific wavelengths of light (quantum-state light at 1550 nm and synchronization light at 1570 nm). Thus, a 1550-nm wavelength laser beam is emitted from a laser diode (LD) and transmitted to the Pass port of the DWDM. Similarly, the TL emits c.w. light with the wavelength at 1570 nm to simulate Alice’s synchronization light. The COM port of the DWDM is connected to the HPL through a 99:1 BS, simulating Eve’s laser damage attack on the transmitter via

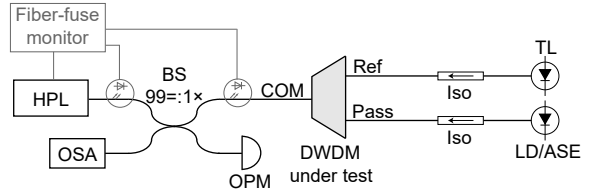


FIG. 8. Schematic diagram of the experimental setup, with the DWDM as a replaceable sample under test. All fibers are standard single mode. OSA, optical spectrum analyzer; OPM, optical power meter; COM, common port; Pass, pass port; Ref, reflect port; TL, tunable laser; LD, laser diode; ASE, amplified spontaneous emission; HPL, high-power laser; Iso, isolator; BS, beam splitter. The coupling ratio of the BS denoted  $99 =: 1 \times$  means that 99% of light passes to the port horizontally opposite in the graphical symbol of the BS, while 1% of light is coupled across to the other port.

the quantum channel. The OPM is used to measure the input power of the HPL injected to through the COM port. The OSA is used to measure the output spectrum at the COM port of the DWDM. To prevent laser damage to the LD and TL during the experiment, isolators are placed between these light sources and DWDM. Additionally, to mitigate the risk of equipment damage due to optical fiber fuse, a fiber fuse monitor is also applied in the setup.

In the experiment, the LD and TL in Fig. 8 remain continuously turned on, emitting light with the wavelengths around 1550 nm and 1570 nm, respectively. The power of the HPL starts at 0 W [54] and increases by approximately 1 W each time, continuously illuminating for up to 10 minutes. Once the spectrum observed on the OSA meets the criteria of a successfully hacked case as defined in Sec. II, the experiment is immediately terminated. If the HPL power increases to the maximum power with no significant change in spectrum, the experiment is also stopped.

To investigate the changes in the optical properties of light at various wavelengths after passing through a laser-damaged DWDM, we designed a wide-spectrum testing using the Pass port as an example. The experimental setup is slightly modified from the previously described configuration, as shown in Fig. 8, with the difference that an amplified spontaneous emission (ASE) source with wavelength range from 1518.6 nm to 1569.4 nm was used instead of LD connected to the Pass port. Using ASE allows one to assess whether DWDM performance under the laser-damage attack varies in the wide range of wavelengths. Moreover, since the focus of this experiment is on light transmitted through the Pass port, the Ref port is left to be unconnected. The wide-spectrum testing follows the same procedure as the one described above, except that the ASE source is activated in place of the LD and TL.

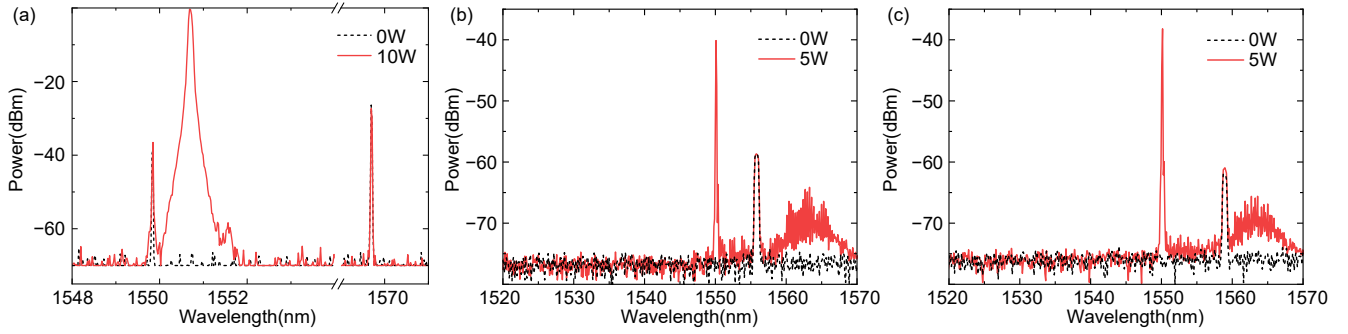


FIG. 9. (a), (b), and (c) show the output spectra at the COM port for samples 8, 9, and 10, respectively, as measured by the OSA. The black dashed curves correspond to the spectra with the HPL turned off, while the red solid curves represent the spectra with the HPL turned on at its maximum output power, respectively.

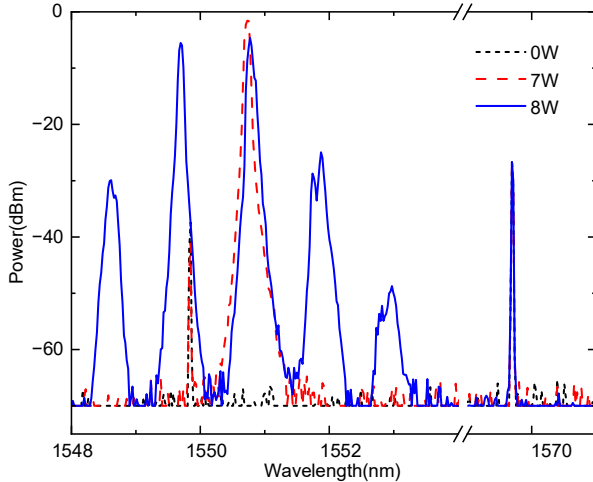


FIG. 10. The experimental results for sample 7. The black dotted line, red dashed line, and blue solid line represent the spectra at the COM port of the DWDM under HPL powers of 0 W, 7 W, and 8 W, respectively.

## 2. Result

In this experiment, four types of DWDM samples (DWDM1, DWDM2, DWDM4, and DWDM5) were tested. Table II presents the detailed parameters of these types of DWDM samples. We used the LD with a wavelength near 1550 nm and conducted the experiment on DWDM1 and DWDM2. For DWDM4 and DWDM5 listed in Table II, we conducted the wide-spectrum testing, i.e., using ASE to replace the LD in order to achieve a broadband spectrum experiment. Among these, only the sample 7 exhibited the successfully hacked case defined in Sec. II, while the other three types of DWDM samples did not show significant change.

For the experiment on sample 7, when the HPL power is set to 0 W, the COM port spectrum exhibits two peaks near 1550 nm and 1570 nm, corresponding to the wavelengths of the incident light from the Pass and Ref ports, respectively. We then measured the COM port spectra

TABLE II. The detailed parameters of the DWDM samples to be tested in experiment

Type	Sample	Central Wavelength(nm)	Manufacturer
DWDM1	7	1550.12	A
DWDM2	8	1550.12	A
DWDM4	9	1555.74	B
DWDM5	10	1558.98	B

with the HPL power set to 1, 2, 3, 4, 5, 6, and 7 W. The spectrum at 7 W is presented as a representative example to illustrate this test procedure. As shown in Fig. 10, when the HPL power reaches 7 W, a new peak appears at 1550.7 nm, which matches the wavelength of the HPL. The power of this peak increases with the HPL power, indicating that it originates from the HPL and is captured by the OSA due to end-face reflections within the transmitter. Comparing the spectra at 0 W and 7 W, we observe that the peaks near 1550 nm and 1570 nm remain nearly unchanged, suggesting that the high-power laser irradiation does not affect the transmission efficiency of the DWDM at the Pass and Ref ports.

When the HPL power increases to 8 W, multiple peaks appear in the 1548–1553 nm range, with intervals of approximately 1 nm. Among them, the peaks at 1550 nm and 1551 nm are the strongest, while the others are weaker and symmetrically distributed. Consistent with the phenomena described in Sec. III, this spectrum exhibits a distinct multi-peak structure. The power of these additional peaks significantly exceeds that of the LD light transmitted through the Pass port, suggesting they originate from end-face reflections induced by HPL irradiation. We hypothesize that this multi-peak generation results from a nonlinear optical process within the DWDM that broadens the single-frequency input into an optical frequency comb.

Figure 9(a) presents the test results of the experiment for the sample 8. When the HPL power is set to 0 W, the spectrum exhibits two peaks, similar to the case of sample 7. As the HPL power increases to 10 W, no spectral

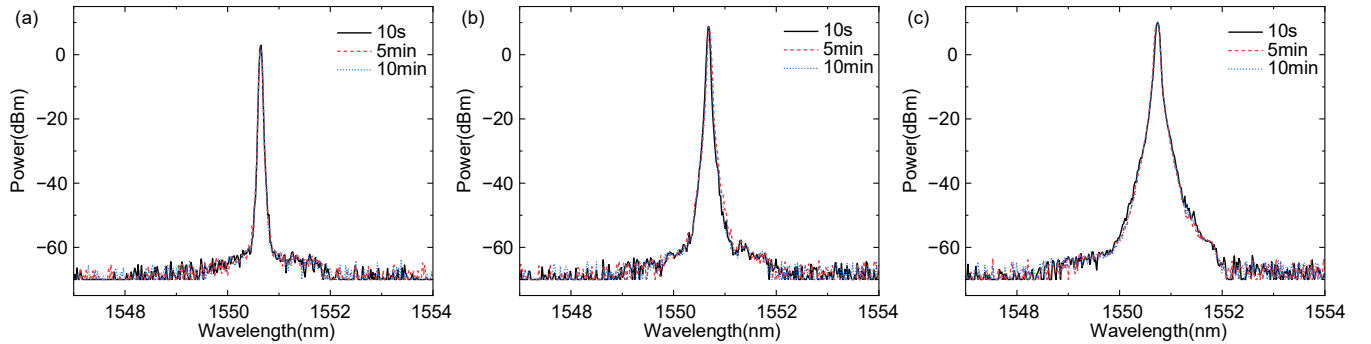


FIG. 11. Stability test results of the HPL. The black solid line, red dashed line, and blue dotted line represent the spectra when the HPL is turned on for 10 seconds, 5 minutes, and 10 minutes, respectively. (a), (b), and (c) correspond to the spectra under HPL powers of 1 W, 5 W, and 10 W, respectively.

changes are observed for the light around 1550 nm and 1570 nm, and the end-face reflection spectrum matches that of the 10 W HPL spectrum shown in Appendix B, with no multi-peak features. This behavior contrasts with that of sample 7 and indicates that the characteristics of sample 8 remain unaffected under the maximum HPL power used.

The results of the wide-spectrum tests for samples 9 and 10 also show no significant changes. In this experiment, the maximum HPL power used was 5 W. As shown in Fig. 9(b) and Fig. 9(c), when the HPL power reaches 5 W, the spectra of both the high-power laser and the ASE source remain essentially unchanged, indicating that samples 9 and 10 preserve their original spectral characteristics under 5 W laser illumination.

#### Appendix B: Details of high-power laser stability test

This section outlines the specifics of the stability test conducted for the HPL, with the test configuration depicted in Fig. 12. In the experimental setup, the HPL is interfaced with OSA1 and OPM1 via a 99:1 BS. OPM1 serves the purpose of measuring the majority of energy emitted by the HPL, while OSA1 is utilized for real-time monitoring and recording of the live spectrum of the HPL to evaluate its stability. Moreover, integration of a fiber fuse monitor ensures immediate deactivation of the HPL upon detection of optical fiber fuse occurrences, thereby safeguarding the equipment from potential damage. OSA1 remains fixed to specific settings throughout the test. The sensitivity level is set at  $-65$  dBm, the scanning rate is  $200$  nm/s, the scanning mode operates in single-scan mode, and the data recording mode runs in live mode. Each instance of OSA1 scanning results in the recording of the spectrum for subsequent analysis.

In order to evaluate the stability of the HPL, tests were conducted to assess its output fluctuation over both short and long durations. The output power of the HPL starts at 1 W and increases incrementally to the maximum value

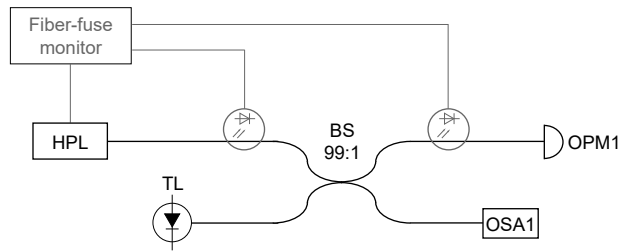


FIG. 12. Schematic diagram of high-power laser stability test.

of 10 W in a linear manner. At each power level, the laser remains continuously active for 10 minutes, during which OSA1 records the real-time output spectrum of the HPL. Fig. 12(a), (b), and (c) show the spectral measurements of the HPL at power levels of 1 W, 5 W, and 10 W, respectively. As seen in the figures, the output spectrum of the HPL remains essentially unchanged over time—at 10 seconds, 5 minutes, and 10 minutes after activation. This indicates that the HPL used in the experiment is highly stable and meets the requirements for conducting the laser-damage attack experiments.

#### Appendix C: Transmitter isolation characterization

To evaluate the transmitter's isolation against Trojan-horse light, we follow the measurement method described in Ref. [50]. Specifically, we use a supercontinuum laser source (NKT Photonics SuperK Fianium FIU-15) and an optical spectrum analyzer (Yokogawa AQ6370D) to measure the broadband transmittance of the optical components. The transmittance of a device under test (DUT) is obtained by first recording the spectrum of the light source alone, followed by a second measurement with the DUT inserted. The DUT transmittance is then calculated as the ratio between the spectral power measured with and without the DUT in place. Using this method, we characterize the broadband transmittance of the attenuator and isolators. The total isolation provided by

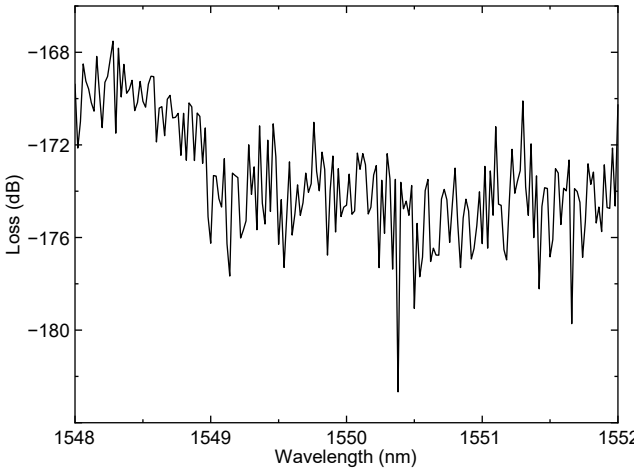


FIG. 13. The total isolation provided by the attenuator and isolators at different wavelengths.

these components at different wavelengths is shown in Fig. 13.

---

[1] C. H. Bennett and G. Brassard, Quantum cryptography: Public key distribution and coin tossing, in *Proc. IEEE International Conference on Computers, Systems, and Signal Processing (Bangalore, India)* (IEEE Press, New York, 1984) pp. 175–179.

[2] N. Gisin, G. Ribordy, W. Tittel, and H. Zbinden, Quantum cryptography, *Rev. Mod. Phys.* **74**, 145 (2002).

[3] V. Scarani, H. Bechmann-Pasquinucci, N. J. Cerf, M. Dušek, N. Lütkenhaus, and M. Peev, The security of practical quantum key distribution, *Rev. Mod. Phys.* **81**, 1301 (2009).

[4] F. Xu, X. Ma, Q. Zhang, H.-K. Lo, and J.-W. Pan, Secure quantum key distribution with realistic devices, *Rev. Mod. Phys.* **92**, 025002 (2020).

[5] V. Makarov, A. Anisimov, and J. Skaar, Effects of detector efficiency mismatch on security of quantum cryptosystems, *Phys. Rev. A* **74**, 022313 (2006).

[6] L. Lydersen, C. Wiechers, C. Wittmann, D. Elser, J. Skaar, and V. Makarov, Hacking commercial quantum cryptography systems by tailored bright illumination, *Nat. Photonics* **4**, 686 (2010).

[7] L. Lydersen, C. Wiechers, C. Wittmann, D. Elser, J. Skaar, and V. Makarov, Thermal blinding of gated detectors in quantum cryptography, *Opt. Express* **18**, 27938 (2010).

[8] F. Xu, B. Qi, and H.-K. Lo, Experimental demonstration of phase-remapping attack in a practical quantum key distribution system, *New J. Phys.* **12**, 113026 (2010).

[9] H.-W. Li, S. Wang, J.-Z. Huang, W. Chen, Z.-Q. Yin, F.-Y. Li, Z. Zhou, D. Liu, Y. Zhang, G.-C. Guo, W.-S. Bao, and Z.-F. Han, Attacking a practical quantum-key-distribution system with wavelength-dependent beam-splitter and multiwavelength sources, *Phys. Rev. A* **84**, 062308 (2011).

[10] C. Wiechers, L. Lydersen, C. Wittmann, D. Elser, J. Skaar, C. Marquardt, V. Makarov, and G. Leuchs, After-gate attack on a quantum cryptosystem, *New J. Phys.* **13**, 013043 (2011).

[11] I. Gerhardt, Q. Liu, A. Lamas-Linares, J. Skaar, C. Kurtseifer, and V. Makarov, Full-field implementation of a perfect eavesdropper on a quantum cryptography system, *Nat. Commun.* **2**, 349 (2011).

[12] N. Jain, C. Wittmann, L. Lydersen, C. Wiechers, D. Elser, C. Marquardt, V. Makarov, and G. Leuchs, Device calibration impacts security of quantum key distribution, *Phys. Rev. Lett.* **107**, 110501 (2011).

[13] A. N. Bugge, S. Sauge, A. M. M. Ghazali, J. Skaar, L. Lydersen, and V. Makarov, Laser damage helps the eavesdropper in quantum cryptography, *Phys. Rev. Lett.* **112**, 070503 (2014).

[14] S.-H. Sun, F. Xu, M.-S. Jiang, X.-C. Ma, H.-K. Lo, and L.-M. Liang, Effect of source tampering in the security of quantum cryptography, *Phys. Rev. A* **92**, 022304 (2015).

[15] S. Sajeed, P. Chaiwongkhot, J.-P. Bourgoin, T. Jennewein, N. Lütkenhaus, and V. Makarov, Security loophole in free-space quantum key distribution due to spatial-mode detector-efficiency mismatch, *Phys. Rev. A* **91**, 062301 (2015).

[16] A. Huang, S. Sajeed, P. Chaiwongkhot, M. Soucarros, M. Legré, and V. Makarov, Testing random-detector-efficiency countermeasure in a commercial system reveals a breakable unrealistic assumption, *IEEE J. of Quantum Electron.* **52**, 1 (2016).

[17] A. Huang, S.-H. Sun, Z. Liu, and V. Makarov, Quantum key distribution with distinguishable decoy states, *Phys. Rev. A* **98**, 012330 (2018).

[18] Y.-J. Qian, D.-Y. He, S. Wang, W. Chen, Z.-Q. Yin, G.-C. Guo, and Z.-F. Han, Hacking the quantum key distribution system by exploiting the avalanche-transition region of single-photon detectors, *Phys. Rev. Appl.* **10**, 064062 (2018).

[19] A. Huang, A. Navarrete, S.-H. Sun, P. Chaiwongkhot, M. Curty, and V. Makarov, Laser-seeding attack in quantum key distribution, *Phys. Rev. Appl.* **12**, 064043 (2019).

[20] A. Huang, R. Li, V. Egorov, S. Tchouragoulov, K. Kumar, and V. Makarov, Laser-damage attack against optical attenuators in quantum key distribution, *Phys. Rev.*

*Appl.* **13**, 034017 (2020).

[21] S. Sun and A. Huang, A review of security evaluation of practical quantum key distribution system, *Entropy* **24**, 260 (2022).

[22] P. Chaiwongkhot, J. Zhong, A. Huang, H. Qin, S.-c. Shi, and V. Makarov, Faking photon number on a transition-edge sensor, *EPJ Quantum Technol.* **9**, 23 (2022).

[23] B. Gao, Z. Wu, W. Shi, Y. Liu, D. Wang, C. Yu, A. Huang, and J. Wu, Ability of strong-pulse illumination to hack self-differencing avalanche photodiode detectors in a high-speed quantum-key-distribution system, *Phys. Rev. A* **106**, 033713 (2022).

[24] A. Ponosova, D. Ruzhetskaya, P. Chaiwongkhot, V. Egorov, V. Makarov, and A. Huang, Protecting fiber-optic quantum key distribution sources against light-injection attacks, *PRX Quantum* **3**, 040307 (2022).

[25] A. Huang, A. Mizutani, H.-K. Lo, V. Makarov, and K. Tamaki, Characterization of state-preparation uncertainty in quantum key distribution, *Phys. Rev. Appl.* **19**, 014048 (2023).

[26] Q. Peng, B. Gao, K. Zaitsev, D. Wang, J. Ding, Y. Liu, Q. Liao, Y. Guo, A. Huang, and J. Wu, Security boundaries of an optical-power limiter for protecting quantum-key-distribution systems, *Phys. Rev. Appl.* **21**, 014026 (2024).

[27] Q. Peng, J.-P. Chen, T. Xing, D. Wang, Y. Wang, Y. Liu, and A. Huang, Practical security of twin-field quantum key distribution with optical phase-locked loop under wavelength-switching attack, *npj Quantum Information* **11**, 7 (2025).

[28] S. Sajeed, A. Huang, S. Sun, F. Xu, V. Makarov, and M. Curty, Insecurity of detector-device-independent quantum key distribution, *Phys. Rev. Lett.* **117**, 250505 (2016).

[29] V. Chistiakov, A. Huang, V. Egorov, and V. Makarov, Controlling single-photon detector id210 with bright light, *Opt. Express* **27**, 32253 (2019).

[30] P. Chaiwongkhot, K. B. Kuntz, Y. Zhang, A. Huang, J.-P. Bourgoin, S. Sajeed, N. Lütkenhaus, T. Jennewein, and V. Makarov, Eavesdropper's ability to attack a free-space quantum-key-distribution receiver in atmospheric turbulence, *Phys. Rev. A* **99**, 062315 (2019).

[31] H. Weier, H. Krauss, M. Rau, M. Fürst, S. Nauerth, and H. Weinfurter, Quantum eavesdropping without interception: an attack exploiting the dead time of single-photon detectors, *New J. Phys.* **13**, 073024 (2011).

[32] L. Lydersen, N. Jain, C. Wittmann, O. Marøy, J. Skaar, C. Marquardt, V. Makarov, and G. Leuchs, Superlinear threshold detectors in quantum cryptography, *Phys. Rev. A* **84**, 032320 (2011).

[33] L. Lydersen, M. K. Akhlaghi, A. H. Majedi, J. Skaar, and V. Makarov, Controlling a superconducting nanowire single-photon detector using tailored bright illumination, *New J. Phys.* **13**, 113042 (2011).

[34] S. Sauge, L. Lydersen, A. Anisimov, J. Skaar, and V. Makarov, Controlling an actively-quenched single photon detector with bright light, *Opt. Express* **19**, 23590 (2011).

[35] H.-K. Lo, M. Curty, and B. Qi, Measurement-device-independent quantum key distribution, *Phys. Rev. Lett.* **108**, 130503 (2012).

[36] V. M. Artem Vakhitov and D. R. Hjelme, Large pulse attack as a method of conventional optical eavesdropping in quantum cryptography, *J. Mod. Opt.* **48**, 2023 (2001).

[37] N. Gisin, S. Fasel, B. Kraus, H. Zbinden, and G. Ribordy, Trojan-horse attacks on quantum-key-distribution systems, *Phys. Rev. A* **73**, 022320 (2006).

[38] N. Jain, E. Anisimova, I. Khan, V. Makarov, C. Marquardt, and G. Leuchs, Trojan-horse attacks threaten the security of practical quantum cryptography, *New J. Phys.* **16**, 123030 (2014).

[39] M. Lucamarini, I. Choi, M. B. Ward, J. F. Dynes, Z. L. Yuan, and A. J. Shields, Practical security bounds against the trojan-horse attack in quantum key distribution, *Phys. Rev. X* **5**, 031030 (2015).

[40] K. Tamaki, M. Curty, and M. Lucamarini, Decoy-state quantum key distribution with a leaky source, *New J. Phys.* **18**, 065008 (2016).

[41] V. Lovic, D. Marangon, P. Smith, R. Woodward, and A. Shields, Quantified effects of the laser-seeding attack in quantum key distribution, *Phys. Rev. Appl.* **20**, 044005 (2023).

[42] P. Ye, W. Chen, G.-W. Zhang, F.-Y. Lu, F.-X. Wang, G.-Z. Huang, S. Wang, D.-Y. He, Z.-Q. Yin, G.-C. Guo, and Z.-F. Han, Induced-photorefraction attack against quantum key distribution, *Phys. Rev. Appl.* **19**, 054052 (2023).

[43] F.-Y. Lu, P. Ye, Z.-H. Wang, S. Wang, Z.-Q. Yin, R. Wang, X.-J. Huang, W. Chen, D.-Y. He, G.-J. Fan-Yuan, G.-C. Guo, and Z.-F. Han, Hacking measurement-device-independent quantum key distribution, *Optica* **10**, 520 (2023).

[44] L. Han, Y. Li, H. Tan, W. Zhang, W. Cai, J. Yin, J. Ren, F. Xu, S. Liao, and C. Peng, Effect of light injection on the security of practical quantum key distribution, *Phys. Rev. Appl.* **20**, 044013 (2023).

[45] Y.-A. Chen, Q. Zhang, T.-Y. Chen, W.-Q. Cai, S.-K. Liao, J. Zhang, K. Chen, J. Yin, J.-G. Ren, Z. Chen, S.-L. Han, Q. Yu, K. Liang, F. Zhou, X. Yuan, M.-S. Zhao, T.-Y. Wang, X. Jiang, L. Zhang, W.-Y. Liu, Y. Li, Q. Shen, Y. Cao, C.-Y. Lu, R. Shu, J.-Y. Wang, L. Li, N.-L. Liu, F. Xu, X.-B. Wang, C.-Z. Peng, and J.-W. Pan, An integrated space-to-ground quantum communication network over 4,600 kilometres, *Nature* **589**, 214 (2021).

[46] C. Clivati, A. Meda, S. Donadello, S. Virzì, M. Genovese, F. Levi, A. Mura, M. Pittaluga, Z. Yuan, A. J. Shields, M. Lucamarini, I. P. Degiovanni, and D. Calonico, Coherent phase transfer for real-world twin-field quantum key distribution, *Nat. Commun.* **13**, 157 (2022).

[47] L. Zhou, J. Lin, Y. Jing, and Z. Yuan, Twin-field quantum key distribution without optical frequency dissemination, *Nat. Commun.* **14**, 928 (2023).

[48] Y. Liu, W.-J. Zhang, C. Jiang, J.-P. Chen, C. Zhang, W.-X. Pan, D. Ma, H. Dong, J.-M. Xiong, C.-J. Zhang, H. Li, R.-C. Wang, J. Wu, T.-Y. Chen, L. You, X.-B. Wang, Q. Zhang, and J.-W. Pan, Experimental twin-field quantum key distribution over 1000 km fiber distance, *Phys. Rev. Lett.* **130**, 210801 (2023).

[49] M. Pittaluga, Y. S. Lo, A. Brzozko, R. I. Woodward, D. Scalcon, M. S. Winnel, T. Roger, J. F. Dynes, K. A. Owen, S. Juárez, P. Rydlichowski, D. Vicinanza, G. Roberts, and A. J. Shields, Long-distance coherent quantum communications in deployed telecom networks, *Nature* **640**, 911 (2025).

[50] V. Makarov, A. Abrikosov, P. Chaiwongkhot, A. K. Fedorov, A. Huang, E. Kiktenko, M. Petrov, A. Ponosova, D. Ruzhetskaya, A. Tayduganov, D. Trefilov, and K. Zaitsev, Preparing a commercial quantum key distribu-

tion system for certification against implementation loop-holes, *Phys. Rev. Appl.* **22**, 044076 (2024).

[51] X. Ma, B. Qi, Y. Zhao, and H.-K. Lo, Practical decoy state for quantum key distribution, *Phys. Rev. A* **72**, 012326 (2005).

[52] D. Gottesman, H.-K. Lo, N. Lutkenhaus, and J. Preskill, Security of quantum key distribution with imperfect devices, in *International Symposium on Information Theory, 2004. ISIT 2004. Proceedings.* (2004) pp. 136–.

[53] H.-K. Lo and J. Preskill, Security of quantum key distribution using weak coherent states with nonrandom phases (2007), [arXiv:quant-ph/0610203 \[quant-ph\]](https://arxiv.org/abs/quant-ph/0610203).

[54] Unlike the experiments presented in the main text, this test starts with an HPL power of 0 W. This is because, in this experiment, other light sources such as the LD are also active. Therefore, when the HPL power is 0 W, the spectrum of the DWDM without the laser-damage attack can still be observed. In contrast, in the main text, only the HPL serves as the light source (with the TL turned off during formal testing). As a result, when the HPL power is 0 W, there is no light source in the setup, making it impossible to measure the DWDM spectrum. Thus, the tests in the main text begin with the HPL power set to 1 W.